

Relaxation of optically excited carriers in graphene: Anomalous diffusion and Lévy flights

U. Briskot,^{1,2} I. A. Dmitriev,^{3,1,2,4} and A. D. Mirlin^{1,2,5}

¹*Institute of Nanotechnology, Karlsruhe Institute of Technology, 76021 Karlsruhe, Germany*

²*Institute for Theoretical Condensed Matter Physics and Center for Functional Nanostructures, Karlsruhe Institute of Technology, 76128 Karlsruhe, Germany*

³*Max Planck Institute for Solid State Research, Heisenbergstr. 1, 70569 Stuttgart, Germany*

⁴*Ioffe Physical Technical Institute, 194021 St. Petersburg, Russia*

⁵*Petersburg Nuclear Physics Institute, 188300 St. Petersburg, Russia*

(Dated: June 13, 2021)

We present a theoretical analysis of the relaxation cascade of a photoexcited electron in graphene in the presence of RPA screened electron-electron interaction. We calculate the relaxation rate of high energy electrons and the jump-size distribution of the random walk constituting the cascade which exhibits fat tails. We find that the statistics of the entire cascade are described by Lévy flights with constant drift instead of standard drift-diffusion in energy space. The Lévy flight manifests nontrivial scaling relations of the fluctuations in the cascade time, which is related to the problem of the first passage time of Lévy processes. Furthermore we determine the transient differential transmission of graphene after an excitation by a laser pulse taking into account the fractional kinetics of the relaxation dynamics.

PACS numbers: 68.65.Pq, 05.40.Fb, 05.45.Df

I. INTRODUCTION

The fabrication of graphene¹ launched a new era of two-dimensional (2D) materials in condensed matter physics, giving access to fundamentally different phenomena and systems realized for the first time in a solid state environment.²⁻⁵ Graphene promises to be an attractive platform for electronic⁶ and in particular optoelectronic applications,⁷⁻⁹ where research reaches from lasing¹⁰ to energy conversion.^{11,12} The nature of interactions and their interplay will limit the intrinsic properties of graphene devices and has therefore attracted interest from the application-oriented as well as fundamental standpoint. For the latter, neutral or intrinsic graphene embodies the paradigm of a marginal Fermi liquid (FL).¹³⁻¹⁵ While graphene in the presence of electron-electron interactions (EEI) establishes a finite Fermi surface at high doping, it crosses over to a relativistic Dirac liquid at lower densities and manifests non-FL relaxation rates¹⁶⁻¹⁸ and transport characteristics.^{6,15,19} Another interesting interaction-dominated transport phenomenon is Coulomb drag in graphene double layer systems²⁰⁻²² which is determined by the peculiar interaction-induced interlayer relaxation.²³⁻²⁸ In the last years it became feasible to examine the interactions even on very short time scales by means of ultra-fast pump-probe measurements.²⁹⁻³¹ They revealed that EEI in graphene dominates over phonon interaction at an early stage of relaxation processes making graphene a highly efficient material for thermoelectric applications.^{32,33} On the other hand the relaxation of high energy electrons follows again a non-FL scheme as electrons relax via a cascade of small steps in energy space.³⁴

So far theoretical work focused on the relaxation rates of thermal electrons using static screening or dy-

namical screening in the random phase approximation (RPA).^{14-19,35-38} Comprehensive numerical studies elucidated the interplay of EEI and phonon interactions^{39,40} as well as the importance of different scattering channels in particular in the context of carrier multiplication via Auger processes.⁴¹ The influence of flexural phonons^{42,43} in free-standing graphene and combined effects of phonons and disorder⁴⁴ have been studied in detail. The relaxation of optically excited carriers in doped graphene^{34,45} was theoretically studied⁴⁶ at zero temperature and is consistent with the cascade picture.

In this work we present an analysis of the relaxation cascade at finite temperature. We consider the first stage of the relaxation process dominated by electron-electron collisions and neglect phonon and disorder effects. In Sec. II we study a single cascade step for undoped as well as for doped graphene in Sec. II and calculate the relaxation rates of high energy electrons in graphene using RPA. The main result of Sec. II is the distribution of the size of a single jump in the random walk describing the relaxation cascade. In Sec. III we infer the characteristics of the whole cascade on the basis of the results presented in Sec. II, with emphasis on the fluctuations on top of the particle's drift in energy space. The cascade process manifest the unique Dirac nature of carriers in graphene as it is described by Lévy flights.⁴⁷ Finally, in Sec. IV we determine the transient differential transmission of a graphene sample after excitation with a laser pulse in the presence of EEI.

II. SINGLE CASCADE STEP

We are going to discuss the relaxation of carriers excited by a laser pulse with central frequency ω_{pump} . We focus

on the dynamics of the excited electrons rather than the questions associated with the equilibration of the low energy thermal electrons. We restrict our analysis to the earliest stage dominated by EEI, in which the energy remains entirely in the electronic system. For moderate pump fluence the phase space density of the excited electrons is much lower than the one of thermal electrons. Scattering and energy relaxation of a high energy excited electron is therefore predominantly due to interaction with thermal electrons. We neglect the mutual scattering of high energy electrons and assume that the low energy electrons remain thermal with temperature T . For small fluences we also neglect the change in T due to illumination. In this sense the excited electrons with an energy of the order $\omega_{\text{pump}}/2$ are relaxing in consecutive steps due to the interaction with a thermal bath of low energy electrons at equilibrium.

In the following we label the eigenstates $|\lambda, \vec{k}\rangle$ of the graphene Hamiltonian $H_0 = v_F \vec{\sigma} \cdot \vec{k}$ with energy $\varepsilon_{\lambda k} = \lambda v_F k$ by the momentum \vec{k} and band index $\lambda = \pm 1$. In the following we set $v_F = \hbar = 1$. We define the relaxation rate via the semiclassical Boltzmann equation

$$\partial_t f_\lambda(\vec{k}) = St[f_\lambda(\vec{k})]. \quad (1)$$

Here $f_\lambda(\vec{k})$ is the occupation of the state $|\lambda, \vec{k}\rangle$. The collision integral $St[f]$ describes the electron-electron scattering. Based on the approximations mentioned above we follow the evolution of a single excited electron starting at momentum \vec{p} as it relaxes due to scattering with the thermal electrons with energies $\varepsilon \ll \varepsilon_p$. We make the ansatz

$$f_\lambda(\vec{k}) = f_T(\lambda k) + \delta f_\lambda(\vec{k}), \quad \delta f_\lambda(\vec{k}) = \delta_{\lambda,+1} \delta_{\vec{k},\vec{p}}. \quad (2)$$

Here $f_T(\varepsilon) = 1/[1 + \exp((\varepsilon - \mu)/T)]$ is the Fermi-Dirac distribution. With the ansatz (2), the relaxation rate of the high energy electron is determined by the outscattering rate in the collision integral,

$$St[f_{+1}(\vec{p})] = - \sum_{2,3,4} W_{12,34} f_3 (1 - f_4) (1 - f_2). \quad (3)$$

In Eq. (3) we used the short-hand notation $i = (\varepsilon_i, \vec{k}_i)$. The transition rate $W_{12,34}$ is given in App. A. Here, we only want to point out that in the case of Dirac particles it contains the overlap of the eigenstates $\langle \lambda_j, \vec{k}_j | \lambda_i, \vec{k}_i \rangle$, that leads to a suppression of backscattering, in addition to the semiclassical matrix element of Coulomb scattering. In terms of the transferred energy ω and momentum q , $\varepsilon_2 = \varepsilon_p - \omega$, $\varepsilon_3 = \varepsilon_4 - \omega$ and $\vec{k}_2 = \vec{p} - \vec{q}$, $\vec{k}_3 = \vec{k}_4 - \vec{q}$, due to the conservation of energy and momentum, see inset in Fig. 1(b).

We can classify the possible scattering processes in terms of interband, $|\omega| > q$ and intraband scattering, $|\omega| < q$. Collinear scattering occurs exactly at $|\omega| = q$.

Combining Eqs. (1) and (3) we obtain an expression for the relaxation rate $\Gamma(p)$ of the photoexcited electron,

defined by the Boltzmann equation

$$\partial_t f_{+1}(\vec{p}) = -\Gamma(p) = St[f_{+1}(\vec{p})], \quad (4)$$

which is written as

$$\Gamma = \int_{-\infty}^{+\infty} d\omega P(\omega). \quad (5)$$

Here $P(\omega)$ is the scattering rate per frequency interval $(\omega, \omega + d\omega)$. On the other hand it defines the distribution of the transferred energy in a single scattering event or cascade step. We thus refer to $P(\omega)$ as the jump-size distribution (JSD) of the relaxation cascade.

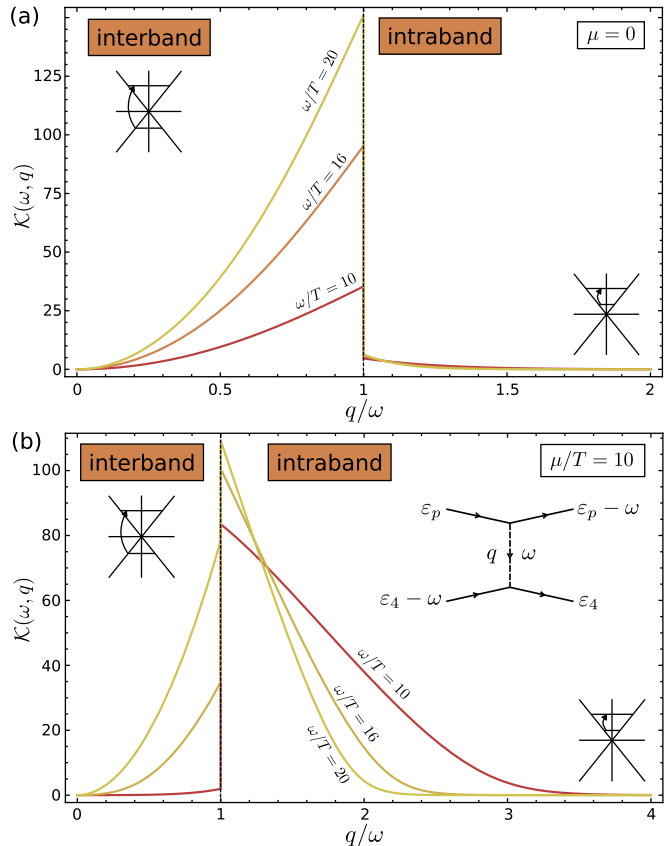


FIG. 1. (Color online) The kernel $\mathcal{K}(\omega, q)$, Eqs. (9) and (C1), determining the phase space of scattering for thermal electrons for different frequencies ω and (a) $\mu = 0$, (b) $\mu/T = 10$. The regions of intraband ($q > |\omega|$) and interband ($q < |\omega|$) scattering are separated by the dashed line.

As long as $\omega < \varepsilon_p$ the excited electron is scattered within the conduction band, which implies $q > |\omega|$. Since the particle number in the conduction and valence band are separately conserved in pair collisions, the thermal electron that scatters with the high energy electron also performs an intraband transition.⁴⁸ We find that the contribution for $\omega > \varepsilon_p$ corresponding to interband transitions is negligible for the relaxation rate Γ , Eqs. (4) and (5), as well as for the statistics of the entire cascade (see Sec. III). Moreover, calculation shows that the relevant

transferred energies satisfy $|\omega| \ll \varepsilon_p$. Scattering in this case is predominantly in forward direction, which simplifies the overlap functions

$$|\langle \lambda_2, \vec{k}_2 | +1, \vec{p} \rangle|^2 = \frac{1 + \lambda_2(\vec{p} \cdot \vec{k}_2)/pk_2}{2} \simeq 1. \quad (6)$$

Taking into account that $f_2 \simeq 0$ for $|\varepsilon_p - \omega| \gg \max(|\mu|, T)$ in Eq. (3), we obtain the compact expression for the JSD,

$$P(\omega) = \int_{|\omega|}^{\infty} dq q \frac{N|V(\omega, q)|^2}{|q^2 - \omega^2|} \mathcal{K}(\omega, q). \quad (7)$$

Here we assumed $\varepsilon_p \gg \max(|\mu|, T)$ and as a consequence $P(\omega)$ is independent of the particle energy ε_p . In Eq. (7) the RPA-screened matrix element of Coulomb scattering

$$V(\omega, q) = V_0(q)/\varepsilon(\omega, q), \quad (8)$$

where the dielectric function $\varepsilon(\omega, q) = 1 + V_0(q)N\Pi(\omega, q)$. The RPA polarization operator $\Pi(\omega, q)$ is given in App. B and the bare Coulomb interaction $V_0(q) = 2\pi\alpha_g/q$. The number of flavors $N = 4$ and the coupling constant in graphene $\alpha_g = e^2/\epsilon\hbar v_F$ in our notations is $\alpha_g = e^2/\epsilon$. Note that in the presence of a dielectric environment with dielectric constant $\epsilon \gg 1$ the coupling constant can be small, $\alpha_g \ll 1$, which we assume in the following. The kernel

$$\mathcal{K}(\omega, q) = \int_{-\infty}^{+\infty} d\varepsilon_4 \sqrt{(\omega - 2\varepsilon_4)^2 - q^2} \times f_T(\varepsilon_4 - \omega)[1 - f_T(\varepsilon_4)], \quad (9)$$

expresses the phase space (for $q > |\omega|$) of the thermal electrons that scatter with the high energy photoexcited electron.

Let us briefly comment on the validity of the RPA. For small frequencies, the RPA sums up the leading logarithmically divergent diagrams.¹⁸ For $|\omega| > \max(T, |\mu|)$, however, the RPA is justified by a large N expansion. By the same degree of approximation we also neglected the exchange term in the collision integral.

We observe that the denominator of the integrand in Eq. (7) is singular in the case of collinear scattering $|\omega| = q$, which in the absence of screening would lead to the logarithmically divergent Coulomb scattering integral.^{15,49,50} However the polarization operator in RPA is also divergent in the case of collinear scattering, thus the total scattering amplitude remains finite. The singular nature of the scattering of Dirac particles with linear dispersion also manifest itself in the phase space kernel (9). Figure 1 shows \mathcal{K} for intrinsic graphene ($|\mu| \ll T$) as well as for $|\mu| \gg T$. In either case \mathcal{K} exhibits a jump at collinear scattering. One observes that for $\mu = 0$ [Fig. 1(a)] the phase space of intraband processes is strongly suppressed and controlled by T . On the contrary, for $|\mu| \gg T$ [Fig. 1(b)] \mathcal{K} is dominated by intraband processes.

Below we discuss the JSD separately for $T \gg |\mu|$ and $|\mu| \gg T$.

A. The limit $T \gg |\mu|$

For $T \gg |\mu|$, there are two important scattering processes. The first one is intraband scattering with small momentum transfer $q < 2T$, which leads to a logarithmic divergence in the JSD for frequencies $|\omega| < \alpha_g T$, depicted as the dash-dotted line in Fig. 2(b). The logarithm occurs due to the failure of screening at small frequencies and momenta which enables resonant forward scattering. It is the only surviving feature of the logarithmic divergence of the unscreened Coulomb scattering integral typical for 2D systems. The contribution of scattering with $q < 2T$ decreases monotonically with increasing frequency and vanishes for $|\omega| \geq 2T$ since $|\omega| > q$ forbids intraband scattering.

The second kind of process is intraband scattering with large momentum transfer $q > 2T$. This contribution increases with increasing frequency up to $\omega = 2T$. It dominates over scattering with small momentum transfer for $\omega \sim 2T$ and higher frequencies. For frequencies $\omega > 2T$ it decreases monotonically. Specifically, we find that at large ω the JSD falls off as $\omega^{-5/2}$, shown in Fig. 2(a). There is a finite probability for the excited electron to gain energy from the bath of thermal electrons. However negative frequencies are exponentially suppressed as shown in Fig. 2(a). The slow decay of the JSD for large frequencies has important implications for the fluctuations of ω as discussed in Sec. III. In particular it is different from the JSD of a FL which is flat in the range $0 < \omega < \varepsilon_p$. Thus an electron in a FL would lose most of its energy by a single jump. The FL regime is realized under the conditions $|\mu| \gg T$ and $\varepsilon_p \ll |\mu|$.

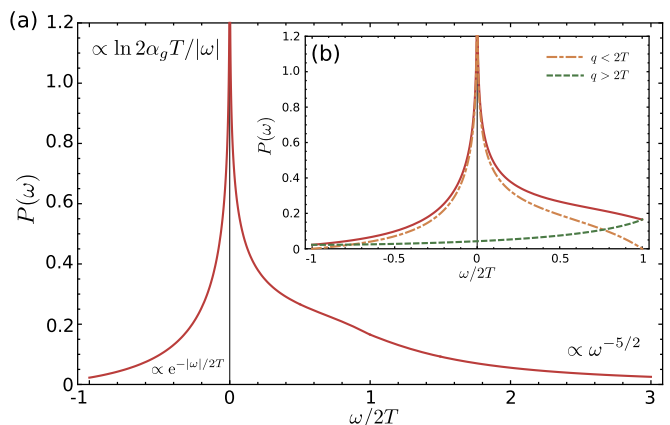


FIG. 2. (Color online) The jump-size distribution (7) for $T \gg |\mu|$. The inset (b) shows the contributions of $q > 2T$ (dashed line) and $q < 2T$ (dash-dotted line) to $P(\omega)$ (solid line) for $|\omega| < 2T$. Both curves are calculated for $\alpha_g = 0.75$.

It turns out that for the scattering rate (5) the region $|\omega| < 2T$ is most important and

$$\Gamma = \kappa\alpha_g T, \quad |\mu| \ll T, \quad \alpha_g \ll 1, \quad (10)$$

where $\kappa = 4\pi^2(1 + \ln 2 + G/2) \simeq 84.92$ and $G \simeq 0.916$ is the Catalan constant. The linear dependence on T

is a characteristic feature of intrinsic graphene that distinguishes it from the FL.¹⁴ Furthermore, due to screening the rate (10) is independent of the number of flavors N and linear in α_g contrary to the golden rule result $\Gamma \propto \alpha_g^2 T$.¹⁸ The rate (10) is also independent of the particle energy $\varepsilon_p \gg \max(|\mu|, T)$.

B. The limit $|\mu| \gg T$

For $|\mu| \gg T$ the JSD is dominated by the region $|\omega| < 2|\mu|$ as can be seen in Fig. 3(a) while the weight of the tail is strongly reduced. In particular the mean jump-size will be of the order $|\mu|$. At the lowest frequencies $|\omega| < \alpha_g T$, the JSD $P(\omega)$ shows a logarithmic divergence due to unscreened collinear scattering. Here the JSD recovers the FL form $P(\omega) \propto (T/|\mu|) \ln |\mu/\omega|$ [see Ref. 16] in contrast to the result for $T \gg |\mu|$, where we obtain $P(\omega) \propto \ln(\alpha_g T/|\omega|)$. In the $T = 0$ limit the logarithmic divergence at small energies vanishes, see Fig. 3(b). In this case $P(\omega)$ reproduces the result of Ref. 46.

The dominant process for $|\omega| < 2|\mu|$ is the intraband scattering with small momentum transfer, $q < 2|\mu|$. Similar to the case $T \gg |\mu|$, such small-momentum scattering is not possible for $\omega > 2|\mu|$ where scattering with $q > 2|\mu|$ leads to the fat tail $\propto \omega^{-5/2}$. The contribution of negative frequencies $P(\omega < 0) \propto \exp(\omega/2T)$ is exponentially small.

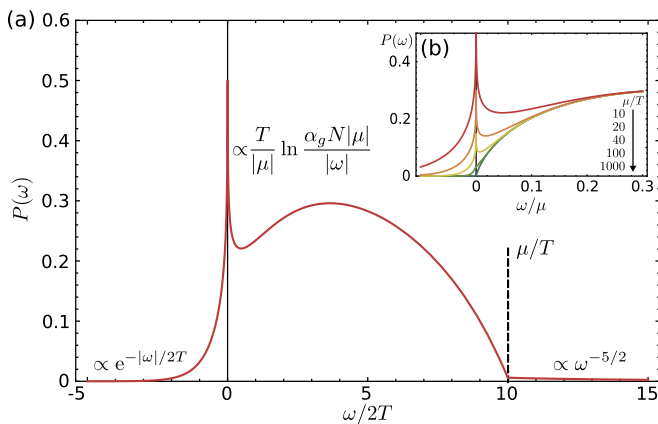


FIG. 3. (Color online) The JSD (7) for $\mu/T = 10$. In the region $|\omega| < 2|\mu|$ processes with $q < 2|\mu|$ are dominant. For $|\omega| > 2|\mu|$ processes with $q > 2|\mu|$ determine the fat tail of the JSD. The inset (b) illustrates the evolution of the forward scattering resonance with lowering temperature. Both curves are calculated for $\alpha_g = 0.75$. For details of the calculation, see App. A.

In the case $T \gg |\mu|$, the relaxation rate was determined by $|\omega| < 2T$. The total rate for $|\mu| \gg T$, is dominated by $0 < \omega < 2|\mu|$ and is given by

$$\Gamma = 8\alpha_g\pi^2|\mu|, \quad |\mu| \gg T, \quad \alpha_g \ll 1. \quad (11)$$

The rates (11) and (10) are calculated in the ballistic regime $T\tau_{\text{dis}} \gg 1$, where we neglect the influence of

disorder with the characteristic scattering time τ_{dis} . In the FL case it is known that the presence of disorder has strong influence on the inelastic relaxation of particles in the diffusive regime $T\tau_{\text{dis}} \ll 1$.^{51–53} However, even in the diffusive regime the tails of the JSD $\propto \omega^{-5/2}$ are preserved for $\omega\tau_{\text{dis}} \gg 1$, since they emerge due to scattering with large momentum transfer.

We finish this section with a short discussion of corrections to the results above due to nonlinearity of the spectrum at high energies $\varepsilon^* \lesssim \Lambda$, where Λ is the cutoff energy. The nonlinear correction to the dispersion relation reads $\varepsilon_\lambda(p) - \lambda k \propto k^2 \sin \varphi_k / \Lambda$, where φ_k is the angle of the direction of \vec{k} . The parameter that controls violations of the linear dispersion relation is therefore ε^* / Λ . Here $\varepsilon^* \sim \omega_{\text{pump}}$ is a characteristic energy. A positive curvature of the spectrum opens a phase space for Auger processes (see Appendix D). Auger processes thus also contribute to the tail of the JSD. From a simple estimate (see Appendix D) we obtain that Auger processes dominate over intraband processes for $\omega \gtrsim T(T^{1/3}\Lambda^{2/3}/\varepsilon^*)^2$. This region is irrelevant if $\varepsilon^* \lesssim \Lambda(T/\Lambda)^{5/9}$. Under this condition the nonlinearity does not modify the tail of $P(\omega)$. For room temperature and the cutoff $\Lambda = 1\text{eV}$, even near-infrared to visible light is within the range of validity of the results of this section. Since positive curvature only occurs in certain directions, Auger processes should be even weaker than in the simple estimate above. We want to stress that a negative curvature prevents Auger processes. Negative curvature appears due to intrinsic band curvature and due to renormalization of the electron spectrum.

III. RELAXATION CASCADE: LÉVY FLIGHTS

We have seen that the JSD of a high energy electron with energy $\varepsilon_p \gg \max(|\mu|, T)$ in graphene implies an average jump size of the order of either temperature or chemical potential. This is in contrast to the FL result where the JSD is flat up to the particle's energy. In graphene, the excited carriers relax in a cascade, with on average $\langle n \rangle \sim \varepsilon_p / \langle \omega \rangle$ jumps, where $\langle \dots \rangle$ is the average according to the JSD. The time scale of the cascade is then $t \sim n/\Gamma$.⁴⁶

The above conclusion concerns the mean number of steps in the cascade as well as the average cascade time. We now discuss the statistics of the random walk modeling the relaxation cascade in more detail with an emphasis on the fluctuations of the number of cascade steps.

Due to the fact that the JSD exhibits the fat tail $P(\omega) \propto \omega^{-5/2}$, it does not possess a second moment. Therefore, the fluctuations of the number of cascade steps should show an unusual behavior. The particle energy provides a natural cutoff for the JSD, rendering its variance finite. But on an intermediate scale, before the electron energy reaches $\max(|\mu|, T)$, the distribution behaves as if it possessed no finite variance. This is demonstrated in Fig. 4(a)-(b) by numerical sampling the JSD [Fig. 4(a)]

and the cascade $S_n = \omega_1 + \dots + \omega_n$ [Fig. 4(b)], where ω_i are independent and identically distributed. For not too large n , a finite cutoff in the JSD does not change the distribution of S_n in Fig. 4(b).

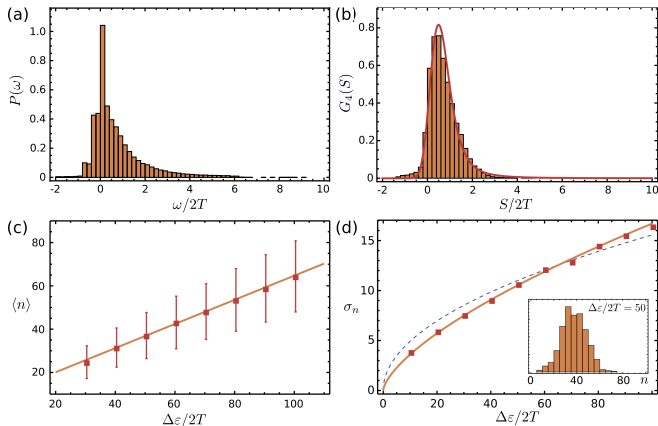


FIG. 4. (Color online) (a) Sample of the JSD for $T \gg |\mu|$ (see Fig. 2). (b) Sample of the cascade variable $S_n = \omega_1 + \dots + \omega_n$ from the JSD for $n = 4$ with a high energy cutoff for the JSD given by the particle energy $\varepsilon_p/T = 100$. The solid line is the stable distribution with $\alpha = 3/2$ and $\beta = 1$. (c) The average number of steps sampled from the JSD as a function of the cascade length $\Delta\varepsilon$. The error bars show the typical fluctuations σ_n of the number of cascade steps. (d) The fluctuation σ_n as a function of the cascade length $\Delta\varepsilon$. The solid line is the $\Delta\varepsilon^{2/3}$ law (19). The dashed line illustrates Gaussian fluctuations for comparison. The inset shows a typical distribution of cascade steps for $\Delta\varepsilon/2T = 50$.

As a consequence, the large- n limit of the distribution of the cascade S_n does not approach the normal distribution. It rather lies in the domain of attraction of an α -stable law $G_n(S_n)$. These are generalized limiting distributions for random processes with stationary and independent jumps including fat-tailed distributions as well as the normal distribution ($\alpha = 2$).⁴⁷ Their characteristic function (excluding the case $\alpha = 1$ irrelevant for us),

$$\Phi_n(\alpha, \delta, \beta, c; z) = e^{izn\delta - nc|z|^\alpha(1 - i\beta\text{sign}(z)\tan(\alpha\pi/2))}, \quad (12)$$

is fully parameterized by four parameters. The index of stability $\alpha = 3/2$ follows from the condition that $G_n(S_n)$ lies in the domain of attraction of an α -stable law,

$$\int_0^x d\omega P(\omega)\omega^2 \propto x^{2-\alpha}, \quad (13)$$

since the large- ω asymptotic of the JSD, $P(\omega)$, is given by

$$P(\omega)T/\Gamma \simeq c(\omega/2T)^{-5/2}. \quad (14)$$

The scale parameter c is obtained from Eqs. (A15) and (A18). It will be related to the anomalous diffusion constant in Sec. IV, Eq. (23). The skewness $\beta = 1$ in the

case of graphene, rendering the distribution single sided - the electron loses energy in the cascade. The location parameter $\delta = \langle\omega\rangle$. For $|\mu| \gg T$ we have $\delta \sim \alpha_g|\mu|$ whereas $\delta \sim \alpha_g T$ for $T \gg |\mu|$.

The random variable $Y = S_n - n\delta$, describing the fluctuations of the cascade, obeys a strictly stable distribution. The random motion on top of the drift during the relaxation processes is thus not the standard Brownian motion but is rather superdiffusive containing long jumps. The associated statistics serves as a fingerprint of the EEI in graphene.

We discuss three important consequences:

(i) The relaxation rate γ_c of the entire cascade is given by the rate Γ divided by the average number of steps. The latter is given by $\varepsilon_p/\langle\omega\rangle$. Thus we obtain

$$\gamma_c \sim \alpha_g^2 \begin{cases} \mu^2/\varepsilon_p, & |\mu| \gg T \\ T^2/\varepsilon_p, & T \gg |\mu| \end{cases}. \quad (15)$$

(ii) Second, the high-energy tail of the JSD $P(\omega^*)$, $\omega^* \gg \max(|\mu|, T)$, gives also the probability density for a secondary electron or hole to be created in the energy interval $\omega^* \lesssim |\varepsilon| \lesssim \omega^* + \max(|\mu|, T)$. More precisely, in the case $\mu \gg T$ ($-\mu \gg T$) only hot electrons (holes) are created with probability density $P(\omega^*)$, while in the case $T \gg |\mu|$ electrons and holes are created with equal probability $P(\omega^*)/2$. Using $P(\omega^*) \ll P(\langle\omega\rangle)$, the probability to create a secondary electron at energy $\varepsilon \sim \omega^*$ during the entire cascade is then given (up to the factor 1/2) by $P(\omega^*)\varepsilon_p/\langle\omega\rangle$. We conclude that the energy scale

$$\omega_0 \sim \begin{cases} T(\varepsilon_p/\alpha_g|\mu|)^{2/5}, & |\mu| \gg T \\ T(\varepsilon_p/\alpha_g T)^{2/5}, & T \gg |\mu| \end{cases}, \quad (16)$$

separates the regions where the density of downstream particles is smaller ($\omega^* < \omega_0$) and larger ($\omega^* > \omega_0$) than the density of secondary particles, see Fig. 5(a)-(b). In the former region the distribution function should show traces of the tail of the JSD accordingly [Fig. 5(a)].⁵⁴

(iii) The third consequence concerns the scaling behavior of fluctuations of the cascade time - the first passage time of the Lévy process on the finite distance $\Delta\varepsilon$ in the energy space - which is directly related to the random variable Y . The distance $\Delta\varepsilon$ can be for instance given by $\Delta\varepsilon = (\omega_{\text{pump}} - \omega_{\text{probe}})/2$, the difference between the excitation and probing frequency, see Fig. 5. We use the scaling of Lévy stable distributions,

$$G_n(S_n) = n^{-1/\alpha} G_1(Y/n^{1/\alpha})|_{\delta=0}, \quad (17)$$

that follows from Eq. (12) and obtain

$$\langle Y^2 \rangle \sim \Delta\varepsilon^{2/\alpha} T^{2(\alpha-1)/\alpha}. \quad (18)$$

The mean square fluctuation of the number of steps is then given by $\sigma_n^2 = \langle n^2 \rangle - \langle n \rangle^2 = \delta^{-2} \langle Y^2 \rangle$ while the fluctuation of the cascade time

$$\sigma_t = \Gamma^{-1} \sigma_n = T^{(\alpha-1)/\alpha} \Delta\varepsilon^{1/\alpha} / \Gamma \langle \omega \rangle. \quad (19)$$

Using Eq. (10) and (11) in Eq. (19) we obtain,

$$\sigma_t \sim \left(\frac{\Delta\varepsilon}{T}\right)^{1/\alpha} \begin{cases} T/\mu^2, & |\mu| \gg T \\ T^{-1}, & T \gg |\mu| \end{cases}. \quad (20)$$

Both for $|\mu| \gg T$ and for $T \gg |\mu|$ we find a nontrivial dependence on $\sigma_t(T)$ determined by the index of stability α . Since $\alpha = 3/2$ in our case, the fluctuations increase $\propto T^{1/3}$ at $T \ll |\mu|$ and decrease $\propto T^{-5/3}$ at $T \gg |\mu|$.

The dependence of the fluctuations in the number of cascade steps n on the length of the cascade $\Delta\varepsilon$ is demonstrated in Figs. 4(c)-(d). Here the cascade is simulated by generating a sequence of steps from the JSD until the cascade length $\Delta\varepsilon$ is reached. The average number of steps $\langle n \rangle$ in Fig. 4(c) scales linearly with the cascade length $\Delta\varepsilon$. On the other hand, the fluctuations of the number of steps σ_n in Fig. 4(d) obey the relation (19).

The exponent of $\Delta\varepsilon$ in the fluctuations σ_t , Eq. (19), is known as the Hurst exponent $H = 1/\alpha$.^{55,56} It is related to the fractal dimension of the random walk $D_f = 2 - H = 4/3$.⁵⁷ The fractal nature of the relaxation cascade in graphene can be understood in terms of a fast one-dimensional backbone of forward scattering augmented by other less efficient channels in the 2D momentum space, similar to the emergence of fractal dimensions in networks.

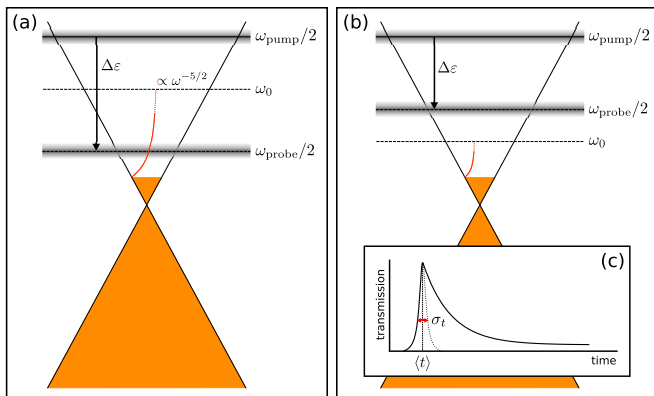


FIG. 5. (Color online) Pump-probe setup for (a) $\omega_{\text{probe}} < \omega_0$: The probe measures mostly the secondary particles which are created with the probability $P(\omega) \propto \omega^{-5/2}$; (b) $\omega_{\text{probe}} > \omega_0$: The density of secondary particles is negligible and the situation is suitable for studying the cascade time and its fluctuations depending on the length of the cascade $\Delta\varepsilon = (\omega_{\text{pump}} - \omega_{\text{probe}})/2$. (c) The fluctuations (19) determine the width of the rise time in the measured change of the transmission [see also the inset of Fig. 4(d)].

IV. FRACTIONAL KINETICS AND TRANSIENT CHANGE IN TRANSMISSION

In this section we will calculate the transient differential transmission of a graphene sample after laser excitation. As in the previous sections we assume that the density of

high energy electrons is much lower than the density of thermal electrons and we can neglect the mutual interaction of the excited carriers. Second, we calculate the isotropic part of the distribution function at high energies $\varepsilon > \omega_0$ [see Fig. 5(b)], thus we can neglect secondary electrons. Furthermore we neglect the exponential tail of the thermal electrons since $\varepsilon \gg \max(|\mu|, T)$. Therefore the isotropic part of the transient distribution function will be given by the distribution of downstream electrons, denoted $F(\varepsilon, t)$.

A. Fractional kinetics

In the previous section we showed that the statistics of the relaxation dynamics is given by Lévy flights. In terms of the distribution function the relaxation will be described by the fractional Fokker-Planck equation (FFPE),⁵⁸

$$\partial_t W(\varepsilon, t) = \Gamma \langle \omega \rangle \partial_\varepsilon W(\varepsilon, t) + D \nabla_{(\beta)}^\alpha W(\varepsilon, t). \quad (21)$$

Here $W(\varepsilon, t)$ with $W(\varepsilon, t = 0) = \delta(\varepsilon)$ is the propagator of the FFPE which will be given below. We also introduced the Riesz-Feller fractional derivative,⁵⁹ which is defined by its Fourier transform,

$$\nabla_{(\beta)}^\alpha f(\varepsilon) = \int \frac{dz}{2\pi} \ln[\Phi_1(\alpha, 0, \beta, 1; z)] f(z) e^{iz\varepsilon}, \quad (22)$$

where Φ_1 is the characteristic function of the underlying stochastic process. In our case it is a Lévy α -stable law with $\alpha = 3/2$ and $\beta = 1$, see Eq. (12). In the FFPE (21) we also introduced the average energy loss rate $\Gamma \langle \omega \rangle$ and the anomalous diffusion constant $D = \Gamma c$, where c is the scale parameter of the Lévy process, see Eqs. (12) and (14). From these formulas we obtain

$$D = \frac{2^\alpha 128 \sqrt{2\pi}}{N/4} T^{\alpha+1}. \quad (23)$$

The emergence of the fractional kinetics expressed by the FFPE (21) can be understood on the basis of a Langevin-type rate equation for the electron energy,

$$\partial_t \varepsilon(t) = -\Gamma \langle \omega \rangle + \eta(t), \quad (24)$$

where $\eta(t)$ is a random variable which is distributed according to an α -stable law and describes the interaction of the high energy electron with the bath of thermal electrons.

The general solution $F(\varepsilon, t)$ of the FFPE with initial conditions $F(\varepsilon, t = 0) = f(\varepsilon)$ is obtained with the propagator according to

$$F(\varepsilon, t) = \int d\varepsilon' W(\varepsilon - \varepsilon', t) f(\varepsilon'). \quad (25)$$

In our case we choose the initial probability density to be

$$f(\varepsilon) = n_0 \delta(\varepsilon - \omega_{\text{pump}}/2). \quad (26)$$

Here n_0 is the integrated flux density of the pump pulse.⁶⁰ We have $F(\varepsilon, t) = n_0 W(\varepsilon, t)$, where

$$\varepsilon_t = \varepsilon - \omega_{\text{pump}}/2 + \Gamma\langle\omega\rangle t, \quad (27)$$

is the running energy. The propagator $W(\varepsilon, t)$ and thus the solution $F(\varepsilon, t)$ in our case of $\alpha = 3/2$ and $\beta = 1$ can be calculated explicitly.⁶¹ We obtain

$$W(\varepsilon, t) = \frac{\pi T}{\alpha} (Dt)^{-1/\alpha} K(s) \quad (28)$$

for the propagator in terms of the dimensionless variable

$$s = \varepsilon_t / (Dt)^{1/\alpha}. \quad (29)$$

In Eq. (28) the function $K(s)$ is given by,

$$K(s) = -e^{\frac{s^3}{27}} \left[\sqrt[3]{2/3} s \text{Ai} \left(\frac{s^2}{\sqrt[3]{486}} \right) + \sqrt[3]{12} \text{Ai}' \left(\frac{s^2}{\sqrt[3]{486}} \right) \right]. \quad (30)$$

Here $\text{Ai}(z)$ is the Airy function and $\text{Ai}'(z)$ its derivative. In particular, W has the following asymptotics for large times,

$$W(\varepsilon, t) \simeq \frac{T D t}{\sqrt{2\pi\alpha}} |\varepsilon - \varepsilon_0 + \Gamma\langle\omega\rangle t|^{-(\alpha+1)}. \quad (31)$$

Using Eq. (23) and the results from Sec. II we obtain,

$$W(\varepsilon, t) \sim t^{-\alpha} \begin{cases} T(T/\mu^2)^{\alpha+1}, & |\mu| \gg T \\ T^{-\alpha}, & T \gg |\mu| \end{cases}. \quad (32)$$

We see that the tail of F for large times but fixed ε is proportional to $t^{-3/2}$ and scales as $T^{-3/2}$ for $T \gg |\mu|$ and as $T(T/\mu^2)^{5/2}$ for $|\mu| \gg T$.

The evolution of the probability distribution $W(\varepsilon, t)$ due to the fractional kinetics is illustrated in Fig. 6. The solid line depicts the solution of the FFPE (21), given by the Eqs. (28)-(30), while the dashed lines show the Gaussian solution of the usual Fokker-Planck equation. The fractional kinetics leads to a strong asymmetry, compared to the Gaussian drift-diffusion, since the fluctuations in the underlying Lévy process are single sided, i.e. $\beta = 1$ in Eq. (12) and (21).

B. Transient change in transmission

We outline the consequences of the fractional kinetics for the transient differential transmission of the sample. The latter is determined by the change in the dynamic conductivity which is given by,

$$\Delta\sigma(t)/\sigma_0 = -[F(\omega_{\text{probe}}/2, t) - F(-\omega_{\text{probe}}/2, t)]. \quad (33)$$

Given the particle hole symmetry of the correction to the distribution function at high energies, i.e. $F(-\varepsilon, t) = -F(\varepsilon, t)$, we finally have for the relative differential transmission

$$\frac{\Delta T(t)}{T_0} = 2n_0 W(\omega_{\text{probe}}/2, t), \quad (34)$$

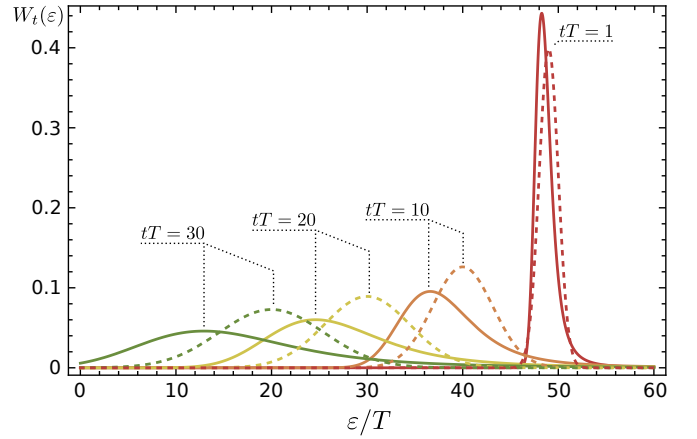


FIG. 6. (Color online) The solution [see Eqs. (28)-(30)] of the FFPE (21) (solid line) as a function of energy in comparison to the result obtained for Gaussian diffusion (dashed line) for different times.

where n_0 is the integrated flux density.

The behavior of ΔT as a function of time, Eq. (34), is illustrated in Fig. 7. The solid line depicts the result (28) due to the fractional kinetics in graphene, while the dashed line is the expected result for conventional Gaussian drift-diffusion. We see that the diffusion in the case of Lévy flights (solid line) is stronger due to the fact that the α -stable law is single sided, i.e. $\beta = 1$. Therefore fluctuations enhance the drift in energy space, see also Fig. 6. Furthermore the transient differential transmission shows powerlaw behavior with time and temperature according to Eq. (32), instead of exponential decay in the case of usual diffusion [see Fig. 7(b)].

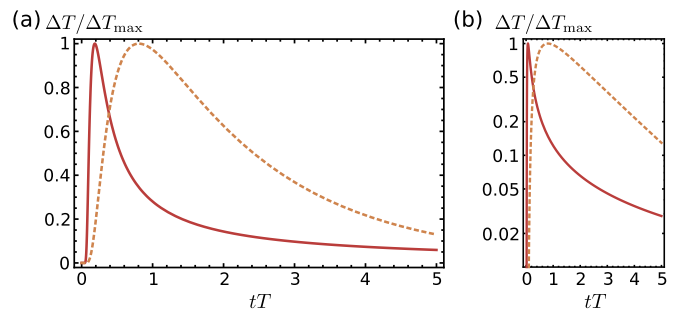


FIG. 7. (Color online) The normalized differential transmission $\Delta T/\Delta T_{\text{max}}$ as a function of the dimensionless time tT . Here ΔT_{max} denotes the maximum value of ΔT . Figure (b) shows the results on a logarithmic scale. The solid curves are calculated according to Eq. (34) and Eqs. (28) and (30), for $\Delta\varepsilon/T = (\omega_{\text{pump}} - \omega_{\text{probe}})/T = 25$ and $\Gamma\langle\omega\rangle/T^2 = 20$ as well as $D/T^{\alpha+1}$ from Eq. (23). The dashed lines in (a) and (b) illustrate the result for usual diffusion in comparison to the fractional kinetics (solid line).

V. CONCLUSION

We have provided an analysis of the relaxation cascade of photoexcited electrons in graphene at finite temperature. We calculated the relaxation rates of high-energy electrons in the case of doped as well as undoped graphene. We find $\Gamma \sim \alpha_g \max(|\mu|, T)$, which distinguishes graphene from the FL. The α_g dependence deviates distinctively from the golden rule result $\propto \alpha_g^2$ and is due to the peculiar screening in graphene.¹⁸ Furthermore the rates are independent of the particle energy ε_p . The entire relaxation cascade is determined by the distribution of the transferred energy in a single jump. This jump-size distribution (JSD) exhibits logarithmic divergencies at small energy transfer due to resonant forward scattering which is very pronounced in graphene having truly linear spectrum. Specifically, we find $P(\omega) \sim \ln \alpha_g T / |\omega|$ for $|\mu| \ll T$ and small frequencies $|\omega| \ll \alpha_g T$ which crosses over into the usual FL result $P(\omega) \sim (T/|\mu|) \ln \alpha_g |\mu/\omega|$ at $|\mu| \gg T$. Remarkably, the JSD exhibits fat tails that fall off as $(\omega/T)^{-5/2}$ at large frequencies $\omega > \max(2|\mu|, 2T)$ for both $|\mu| \gg T$ and $T \gg |\mu|$.

Owing to the fat-tailed JSD, the relaxation cascade is described by an α -stable distribution with a mean drift determined by either T or $|\mu|$: The fluctuations on top of the drift is described by Lévy flights with index of stability $\alpha = 3/2$. As a consequence, the fluctuations σ_t of the cascade time t exhibit characteristic scaling relations with the frequency $\omega_{\text{pump}} \gg \omega_{\text{probe}}$ of the pump pulse, $\sigma_t \sim \omega_{\text{pump}}^{1/\alpha}$, as well as temperature. Specifically, $\sigma_t \sim T^{1/3}$ for $|\mu| \gg T$ and $\sigma_t \sim T^{-5/3}$ for $T \gg |\mu|$. These scaling relations serve a clear imprint of the forward scattering resonance and related fractal nature of the relaxation cascade in graphene. The observed³⁴ variation of the average cascade time with ω_{pump} is consistent with theoretical predictions for the energy drift made in Ref. 46 for the regime $|\mu| \gg T$. Using the experimental setup similar to that used in Refs. 34 and 45, it should be possible to detect the traces of the Lévy flights as well. Specifically, the width of the rise time in the measured change in transmission as depicted in Fig. 5(c) provides a direct measure of the fluctuation of the cascade time

(20) [see also Fig. 4(d)].

Furthermore, the JSD is the distribution of the created electron-hole pairs during the cascade. We find that within the energy window $\max(|\mu|, T) \ll \varepsilon < \omega_0$ a significant amount of secondary electrons are created according to $P(\omega) \simeq \omega^{-5/2}$. We find $\omega_0 \sim T(\omega_{\text{pump}}/T)^{2/5}$ for $T \gg |\mu|$ and $\omega_0 \sim T(\omega_{\text{pump}}/\mu)^{2/5}$ for $|\mu| \gg T$. Probes in the mentioned energy interval should also reveal the tail of the JSD.

We predict the time evolution of the differential change in transmission in the presence of electron electron interactions. The transmission is directly measured in pump probe experiments and we obtain an analytical expression for the differential transmission from a fractional Fokker-Planck equation. The latter is suited to capture the fractional kinetics emerging from the Lévy flight statistics of the relaxation process.

The results of this work extend the study of relaxation dynamics of thermal electrons in graphene¹⁸ to the case of high energy electrons also at finite chemical potential and should be relevant for future studies of the nonequilibrium steady states in irradiated graphene. This prospect includes the question of thermalization in driven graphene, the possibility of a population inversion^{10,62} as well as frequency conversion.⁷ It should also be interesting to extend it to the non-linear regime of pumping where saturation effects become important. All these questions necessitate the full solution of the kinetic equation. In this context the present work sheds new light on the unique character of the interaction in graphene that controls the formation of such nonequilibrium states, that might also be probed in future experiments.

ACKNOWLEDGMENTS

We would like to thank I. Gornyi, B. Jeevanesan, M. Schütt and C. Seiler for useful discussions. Furthermore we are indebted to F. Koppens and K.-J. Tielrooij for discussions and providing insights into experiments.

This work was supported by DFG in the framework of the SPP 1459 and by BMBF.

¹ K. S. Novoselov, A. K. Geim, S. V. Morozov, D. Jiang, Y. Zhang, S. V. Dubonos, I. V. Grigorieva, and A. A. Firsov, *Science* **306**, 666 (2004).
² Y. Zhang, Y.-W. Tan, H. L. Stormer, and P. Kim, *Nature* **438**, 201 (2005).
³ K. S. Novoselov, E. McCann, S. V. Morozov, V. I. Fal'ko, M. I. Katsnelson, U. Zeitler, D. Jiang, F. Schedin, and A. K. Geim, *Nature Physics* **2**, 177 (2006).
⁴ K. Bolotin, K. Sikes, Z. Jiang, M. Klima, G. Fudenberg, J. Hone, P. Kim, and H. Stormer, *Solid State Communications* **146**, 351 (2008).
⁵ X. Du, I. Skachko, A. Barker, and E. Y. Andrei, *Nature*

Nanotechnology **3**, 491 (2008).
⁶ A. H. Castro Neto, F. Guinea, N. M. R. Peres, K. S. Novoselov, and A. K. Geim, *Rev. Mod. Phys.* **81**, 109 (2009).
⁷ F. Bonaccorso, Z. Sun, T. Hasan, and A. C. Ferrari, *Nature Photonics* **4**, 611 (2010).
⁸ P. Avouris, *Nano Letters* **10**, 4285 (2010).
⁹ M. Engel, M. Steiner, A. Lombardo, A. C. Ferrari, H. v. Löhneysen, P. Avouris, and R. Krupke, *Nat. Commun.* **3**, 906 (2012).
¹⁰ T. Li, L. Luo, M. Hupalo, J. Zhang, M. C. Tringides, J. Schmalian, and J. Wang, *Phys. Rev. Lett.* **108**, 167401

- (2012).
- ¹¹ N. M. Gabor, J. C. W. Song, Q. Ma, N. L. Nair, T. Taychatanapat, K. Watanabe, T. Taniguchi, L. S. Levitov, and P. Jarillo-Herrero, *Science* **334**, 648 (2011).
 - ¹² J. C. W. Song, M. S. Rudner, C. M. Marcus, and L. S. Levitov, *Nano Letters* **11**, 4688 (2011).
 - ¹³ D. E. Sheehy and J. Schmalian, *Phys. Rev. Lett.* **99**, 226803 (2007).
 - ¹⁴ J. González, F. Guinea, and M. A. H. Vozmediano, *Phys. Rev. Lett.* **77**, 3589 (1996).
 - ¹⁵ L. Fritz, J. Schmalian, M. Müller, and S. Sachdev, *Phys. Rev. B* **78**, 085416 (2008).
 - ¹⁶ S. Das Sarma, E. H. Hwang, and W.-K. Tse, *Phys. Rev. B* **75**, 121406 (2007).
 - ¹⁷ E. H. Hwang and S. Das Sarma, *Phys. Rev. B* **75**, 205418 (2007).
 - ¹⁸ M. Schütt, P. M. Ostrovsky, I. V. Gornyi, and A. D. Mirlin, *Phys. Rev. B* **83**, 155441 (2011).
 - ¹⁹ A. B. Kashuba, *Phys. Rev. B* **78**, 085415 (2008).
 - ²⁰ S. Kim, I. Jo, J. Nah, Z. Yao, S. K. Banerjee, and E. Tutuc, *Phys. Rev. B* **83**, 161401 (2011).
 - ²¹ R. V. Gorbachev, A. K. Geim, M. I. Katsnelson, K. S. Novoselov, T. Tudorovskiy, I. V. Grigorieva, A. H. MacDonald, S. V. Morozov, K. Watanabe, T. Taniguchi, and L. A. Ponomarenko, *Nature Physics* **8**, 896 (2012).
 - ²² M. Titov, R. V. Gorbachev, B. N. Narozhny, T. Tudorovskiy, M. Schütt, P. M. Ostrovsky, I. V. Gornyi, A. D. Mirlin, M. I. Katsnelson, K. S. Novoselov, A. K. Geim, and L. A. Ponomarenko, *Phys. Rev. Lett.* **111**, 166601 (2013).
 - ²³ W.-K. Tse, B. Y.-K. Hu, and S. Das Sarma, *Phys. Rev. B* **76**, 081401 (2007).
 - ²⁴ M. I. Katsnelson, *Phys. Rev. B* **84**, 041407 (2011).
 - ²⁵ B. N. Narozhny, M. Titov, I. V. Gornyi, and P. M. Ostrovsky, *Phys. Rev. B* **85**, 195421 (2012).
 - ²⁶ J. Lux and L. Fritz, *Phys. Rev. B* **86**, 165446 (2012).
 - ²⁷ J. C. W. Song and L. S. Levitov, *Phys. Rev. Lett.* **111**, 126601 (2013).
 - ²⁸ M. Schütt, P. M. Ostrovsky, M. Titov, I. V. Gornyi, B. N. Narozhny, and A. D. Mirlin, *Phys. Rev. Lett.* **110**, 026601 (2013).
 - ²⁹ D. Sun, Z.-K. Wu, C. Divin, X. Li, C. Berger, W. A. de Heer, P. N. First, and T. B. Norris, *Phys. Rev. Lett.* **101**, 157402 (2008).
 - ³⁰ J. M. Dawlaty, S. Shivaraman, M. Chandrashekar, F. Rana, and M. G. Spencer, *Appl. Phys. Lett.* **92**, 042116 (2008).
 - ³¹ S. Winnerl, F. Göttfert, M. Mittendorff, H. Schneider, M. Helm, T. Winzer, E. Malic, A. Knorr, M. Orlita, M. Potemski, M. Sprinkle, C. Berger, and W. A. de Heer, *Journal of Physics: Condensed Matter* **25**, 054202 (2013).
 - ³² M. Breusing, C. Ropers, and T. Elsaesser, *Phys. Rev. Lett.* **102**, 086809 (2009).
 - ³³ J. Shang, Z. Luo, C. Cong, J. Lin, T. Yu, and G. G. Gurzadyan, *Appl. Phys. Lett.* **97**, 163103 (2010).
 - ³⁴ K. J. Tielrooij, J. C. W. Song, S. A. Jensen, A. Centeno, A. Pesquera, A. Zurutuza Elorza, M. Bonn, L. S. Levitov, and F. H. L. Koppens, *Nature Physics* **9**, 248 (2013).
 - ³⁵ E. H. Hwang, B. Y.-K. Hu, and S. Das Sarma, *Phys. Rev. B* **76**, 115434 (2007).
 - ³⁶ M. Polini, R. Asgari, Y. Barlas, T. Pereg-Barnea, and A. MacDonald, *Solid State Communications* **143**, 58 (2007).
 - ³⁷ M. Polini, R. Asgari, G. Borghi, Y. Barlas, T. Pereg-Barnea, and A. H. MacDonald, *Phys. Rev. B* **77**, 081411 (2008).
 - ³⁸ M. R. Ramezanali, M. M. Vazifeh, R. Asgari, M. Polini, and A. H. MacDonald, *J. Phys. A: Math. Theor.* **42**, 214015 (2009).
 - ³⁹ M. Breusing, S. Kuehn, T. Winzer, E. Malić, F. Milde, N. Severin, J. P. Rabe, C. Ropers, A. Knorr, and T. Elsaesser, *Phys. Rev. B* **83**, 153410 (2011).
 - ⁴⁰ R. Kim, V. Perebeinos, and P. Avouris, *Phys. Rev. B* **84**, 075449 (2011).
 - ⁴¹ A. Tomadin, D. Brida, G. Cerullo, A. C. Ferrari, and M. Polini, *Phys. Rev. B* **88**, 035430 (2013).
 - ⁴² E. Mariani and F. von Oppen, *Phys. Rev. Lett.* **100**, 076801 (2008); F. von Oppen, F. Guinea, and E. Mariani, *Phys. Rev. B* **80**, 075420 (2009).
 - ⁴³ I. V. Gornyi, V. Y. Kachorovskii, and A. D. Mirlin, *Phys. Rev. B* **86**, 165413 (2012).
 - ⁴⁴ J. C. W. Song, M. Y. Reizer, and L. S. Levitov, *Phys. Rev. Lett.* **109**, 106602 (2012).
 - ⁴⁵ D. Brida, A. Tomadin, C. Manzoni, Y. J. Kim, A. Lombardo, S. Milana, R. R. Nair, K. S. Novoselov, A. C. Ferrari, G. Cerullo, and M. Polini, *Nat Commun* **4**, 1987 (2013).
 - ⁴⁶ J. C. W. Song, K. J. Tielrooij, F. H. L. Koppens, and L. S. Levitov, *Phys. Rev. B* **87**, 155429 (2013).
 - ⁴⁷ W. Feller, *An introduction to probability theory and its applications*, 2nd ed., Vol. 2: (Wiley, New York, NY, 1971).
 - ⁴⁸ M. S. Foster and I. L. Aleiner, *Phys. Rev. B* **79**, 085415 (2009).
 - ⁴⁹ E. M. Lifshitz and L. P. Pitaevskii, *Course of theoretical physics*, reprint. ed., edited by J. B. Sykes, Vol. 10: Physical kinetics (1997).
 - ⁵⁰ S. Sachdev, *Phys. Rev. B* **57**, 7157 (1998).
 - ⁵¹ A. Schmid, *Z. Phys.* **271**, 251 (1974).
 - ⁵² B. L. Al'tshuler and G. Aronov, *JETP Lett.* **30**, 482 (1979).
 - ⁵³ E. Abrahams, P. W. Anderson, P. A. Lee, and T. V. Ramakrishnan, *Phys. Rev. B* **24**, 6783 (1981).
 - ⁵⁴ In fact secondary electrons generated during the cascade will also relax. The account for this relaxation requires the full solution of the kinetic equation which is beyond the scope of this work.
 - ⁵⁵ H. E. Hurst, *Trans. Am. Soc. Civ. Eng.* **116**, 770 (1951).
 - ⁵⁶ H. C. Fogedby, T. Bohr, and H. J. Jensen, *Journal of Stat. Phys.* **66**, 583 (1992).
 - ⁵⁷ J. Feder, *Fractals*, Physics of solids and liquids (Plenum Pr., New York, 1988).
 - ⁵⁸ S. Jespersen, R. Metzler, and H. C. Fogedby, *Phys. Rev. E* **59**, 2736 (1999).
 - ⁵⁹ F. Mainardi, G. Pagnini, and R. Saxena, *Journal of Computational and Applied Mathematics* **178**, 321 (2005).
 - ⁶⁰ For a Gaussian initial density $f(\varepsilon) = (n_0/\delta\sqrt{2\pi}) \exp[(\varepsilon - \omega_{\text{pump}}/2)^2/2\delta^2]$ with width δ , our results remain valid for large times $t \gg \delta^\alpha/D$, when the initial condition is washed out and the form of the probability density is determined by diffusion.
 - ⁶¹ The propagator can be written for arbitrary α and β in terms of the Fox H-function.
 - ⁶² V. Ryzhii, M. Ryzhii, and T. Otsuji, *J. Appl. Phys.* **101**, 083114 (2007).

Appendix A: Calculation of the relaxation rate and the JSD from the Boltzmann equation

In this section we derive Eq. (7) for the JSD and the relaxation rates from the main text. We start from a generic fermionic collision integral

$$St[f(\lambda, \vec{p})] = \sum_{\lambda_3} \int \frac{d^2 p_3}{(2\pi)^2} \left\{ W(\lambda, \vec{p} | \lambda_3, \vec{p}_3) f_{\lambda_3}(\vec{p}_3) [1 - f_\lambda(\vec{p})] - W(\lambda_3, \vec{p}_3 | \lambda, \vec{p}) f_\lambda(\vec{p}) [1 - f_{\lambda_3}(\vec{p}_3)] \right\}, \quad (\text{A1})$$

where the transition rates for the Coulomb interaction

$$W(\vec{p}_2, \lambda_2 | \vec{p}_1, \lambda_1) = (2\pi)^{-1} \sum_{\lambda_3, \lambda_4} \int d\vec{p}_{3,4} \int d\vec{q} d\omega \delta(\lambda_2 p_2 + \omega - \lambda_1 p_1) \delta(\lambda_4 p_4 - \omega - \lambda_3 p_3) \times \delta(\vec{p}_2 + \vec{q} - \vec{p}_1) \delta(\vec{p}_4 - \vec{q} - \vec{p}_3) K(\vec{q}, \omega, \{\lambda_i\}, \{\vec{v}_i\}) f(\vec{p}_3, \lambda_3) [1 - f(\vec{p}_4, \lambda_4)]. \quad (\text{A2})$$

Here the interaction kernel

$$K(q, \omega, \{\lambda_i\}, \{\mathbf{v}_i\}) = N |V(\omega, q)|^2 \Theta_{1,2} \Theta_{3,4}, \quad (\text{A3})$$

contains the RPA screened Coulomb matrix element (see App. B)

$$|V(\omega, q)|^2 = \frac{4\pi^2 \alpha_g^2}{(q + 2\pi \alpha_g N \text{Re}\Pi)^2 + (2\pi \alpha_g N \text{Im}\Pi)^2}, \quad (\text{A4})$$

as well as the Dirac factors ($\vec{v}_i = \lambda_i \vec{k}_i / k_i$) $\Theta_{1,2} = (1 + \vec{v}_1 \cdot \vec{v}_2)/2$. Upon inserting the ansatz (2) into the collision integral (A1), we obtain the explicit expression for the relaxation rate

$$\Gamma = \sum_{\lambda_1} \int \frac{d^2 k}{(2\pi)^2} W_0(\lambda_1, \vec{k} | +1, \vec{p}) [1 - f_{\lambda_1}(\vec{k})] + W_0(+1, \vec{p} | \lambda_1, \vec{k}) f_{\lambda_1}(\vec{k}). \quad (\text{A5})$$

For $\omega < \varepsilon_p$, where interband processes are forbidden, the second term in Eq. (A6) can be dropped. Using Eqs. (A2)-(A3) we then obtain

$$\Gamma = (2\pi)^2 \sum_{\lambda_{1,3,4}} \int \frac{d^2 q}{(2\pi)^2} \frac{d\omega}{2\pi} \frac{d^2 k_4}{(2\pi)^2} \delta(\lambda_2 |\vec{p} - \vec{q}| + \omega - p) \delta(\lambda_4 k_4 - \omega - \lambda_3 |\vec{k}_4 - \vec{q}|) \times N |V_{RPA}(\omega, q)|^2 \Theta_{1,2} |_{1=(\lambda_1, \vec{p}-\vec{q})} \Theta_{3,4} |_{3=(\lambda_3, \vec{k}_4-\vec{q})} f_T(\lambda_4 k_4 - \omega) [1 - f_T(\lambda_4 k_4)]. \quad (\text{A6})$$

Next we perform the angular integration in the integrals over \vec{k}_4 and \vec{q} . The arising functional determinants are ($\lambda = +1$),

$$\left| \frac{\partial}{\partial \varphi_q} \lambda_2 |\vec{p} - \vec{q}| \right| = \frac{pq |\sin(\varphi_q - \varphi_p)|}{|\vec{p} + \vec{q}|} = \frac{\sqrt{q^2 - \omega^2} [(\omega - 2\lambda p)^2 - q^2]^{1/2}}{2|\lambda p - \omega|}, \quad (\text{A7})$$

$$\left| \frac{\partial}{\partial \varphi_4} \lambda_3 |\vec{k}_4 - \vec{q}| \right| = \frac{k_4 q |\sin(\varphi_4 - \varphi_q)|}{|\vec{k}_4 - \vec{q}|} = \frac{\sqrt{q^2 - \omega^2} [(\omega - 2\lambda_4 k_4)^2 - q^2]^{1/2}}{2|\lambda_4 k_4 - \omega|}. \quad (\text{A8})$$

The corresponding Dirac factors are ($\lambda_1 = \lambda = +1$)

$$\Theta_{1,2} = \frac{1}{2} \left(1 + \frac{\lambda_1 \lambda_2 \vec{k}_1 \cdot (\vec{p} - \vec{q})}{k_1 |\vec{p} - \vec{q}|} \right) = \frac{|(\omega - 2\lambda p)^2 - q^2|}{4p |\lambda p - \omega|}, \quad (\text{A9})$$

$$\Theta_{3,4} = \frac{1}{2} \left(1 + \frac{\lambda_2 \lambda_3 \vec{k}_4 \cdot (\vec{k}_4 - \vec{q})}{k_4 |\vec{k}_4 - \vec{q}|} \right) = \frac{|(\omega - 2\lambda_4 k_4)^2 - q^2|}{4k_4 |\lambda_4 k_4 - \omega|}. \quad (\text{A10})$$

1. The JSD $P(\omega)$

Putting together Eqs. (A6)-(A10) we finally obtain the JSD

$$P(\omega) = \int_0^\infty dq \frac{q \operatorname{Re} \sqrt{\operatorname{sign}(q^2 - \omega^2)[(\omega - 2\lambda p)^2 - q^2]}}{2p} \frac{N|V(\omega, q)|^2}{|q^2 - \omega^2|} \mathcal{K}(\omega, q). \quad (\text{A11})$$

Here the kinetic kernel is given by Eq. (C1). If we assume $p \gg \omega, q$ we obtain the result (7) stated in the main text,

$$P(\omega) = \int_{|\omega|}^\infty dq q \frac{N|V(\omega, q)|^2}{|q^2 - \omega^2|} \mathcal{K}(\omega, q). \quad (\text{A12})$$

In the following we use the dimensionless variables $\Omega = \omega/2T$, $Q = q/2T$, $\beta = \omega/q$ and $\tilde{\mu} = \mu/T$. Using the asymptotics from App. B and C we obtain limiting expressions for the JSD $P(\Omega)$ presented below.

a. The limit $T \gg |\mu|$ for $|\Omega| < 1$

The contribution for small momentum transfer ($Q < 1$) reads,

$$P(\Omega)|_{Q < 1} = 4 \ln 2 \alpha_g^2 \pi^2 N e^\Omega \int_{|\Omega|}^1 dQ \frac{Q}{|Q^2 - \Omega^2|(Q + \alpha_g N \ln 2)^2 + (\alpha_g N \ln 2\Omega)^2} = \frac{4\pi^2}{N \ln 2} \ln \frac{\alpha_g N \ln 2}{|\Omega|}. \quad (\text{A13})$$

Here the last equality is valid for $|\Omega| < \alpha_g N \ln 2$. The contribution to the JSD with large momentum transfer ($Q > 1$) for frequencies $|\Omega| < 1$ is,

$$P(\Omega)|_{Q > 1} = 2\alpha_g^2 \pi^2 N e^\Omega \int_1^\infty dQ \frac{\sqrt{2\pi} Q^{3/2} e^{-Q}}{(\sqrt{Q^2 - \Omega^2} Q + \alpha_g \pi N Q^2/16)^2 + (\alpha_g \pi N e^{-Q} \sqrt{Q/2\pi})^2}. \quad (\text{A14})$$

The latter can be neglected for $|\Omega| < \alpha_g$.

b. The limit $T \gg |\mu|$ for $|\Omega| > 1$ ($Q > 1$)

For $|\Omega| > 1$, where only intraband transitions with $Q > 1$ are possible, the JSD reads,

$$P(\Omega) = 2\alpha_g^2 \pi^2 N e^\Omega \int_{|\Omega|}^\infty dQ \frac{\sqrt{2\pi} Q^{3/2} e^{-Q}}{(\sqrt{Q^2 - \Omega^2} Q + \alpha_g \pi N Q^2/16)^2 + (\alpha_g \pi N e^{-Q} \sqrt{Q/2\pi})^2} \simeq \frac{2^9 \sqrt{2\pi}}{N} |\Omega|^{-5/2}, \quad (\text{A15})$$

where the asymptotics is valid for $|\Omega| \gg 1$.

c. The limit $|\mu| \gg T$ for $|\Omega| < |\tilde{\mu}|$ ($Q < |\tilde{\mu}|$)

$$P(\Omega) = 4\alpha_g^2 \pi^2 N \Omega |\tilde{\mu}| (1 + \coth(\Omega)) \int_{|\Omega|}^{|\tilde{\mu}|} dQ \frac{Q}{(Q^2 - \Omega^2)(Q + \alpha_g N |\tilde{\mu}|/2)^2 + (\alpha_g N \tilde{\mu} \Omega/2)^2}. \quad (\text{A16})$$

Equation (A16) can be integrated analytically, similar to Eq. (A13), yielding a lengthy expression. For brevity we give the limit for $|\Omega| \ll \alpha_g |\mu|$,

$$P(\Omega) \simeq \frac{1}{32\pi} \frac{\ln \alpha_g N |\mu/2\Omega|}{|\mu|^2}. \quad (\text{A17})$$

d. The limit $|\mu| \gg T$ for $|\Omega| > |\tilde{\mu}|$ ($Q > |\tilde{\mu}|$)

As in the case $|\tilde{\mu}| \ll 1$, here for $|\Omega| > |\tilde{\mu}|$ the JSD is determined by scattering with large momentum transfer,

$$P(\Omega) = 2\alpha_g^2 \pi^2 N e^{+\Omega} \int_{|\Omega|}^\infty dQ \frac{\sqrt{2\pi} Q^{3/2} e^{-Q}}{(\sqrt{Q^2 - \Omega^2} Q + \alpha_g \pi N Q^2/16)^2} \simeq \frac{2^9 \sqrt{2\pi}}{N} |\Omega|^{-5/2}. \quad (\text{A18})$$

2. The relaxation rate Γ

a. *The limit $T \gg |\mu|$*

We first calculate the relaxation rate for $T \gg |\mu|$. We find that the contribution from the region with $Q > 1$ is of order α_g^2 , whereas $|\Omega| < 1$ yields the leading contribution $\propto \alpha_g$:

$$\Gamma/2T = \int_0^{\alpha_g N \ln 2} d\Omega P(\Omega)|_{Q < 1} + \int_{\alpha_g N \ln 2}^1 d\Omega P(\Omega)|_{Q < 1}. \quad (\text{A19})$$

Here, $P(\Omega)|_{Q < 1}$ is given by Eq. (A13) and we anticipate that the integrand contains the scale $\alpha_g N \ln 2$ that separates the logarithmic divergence at small frequency from the rest. The first part in Eq. (A19) yields,

$$\begin{aligned} \int_0^{\alpha_g N \ln 2} d\Omega P(\Omega)|_{Q < 1} &= 4 \ln 2 \alpha_g^2 \pi^2 N \int_0^{\alpha_g N \ln 2} d\Omega \left\{ \frac{1}{(\alpha_g N \ln 2)^2} \ln \frac{\alpha_g N \ln 2}{|\Omega|} + \int_{\alpha_g N \ln 2}^1 dQ \frac{1}{Q(Q^2 - \Omega^2)} \right\} \\ &= 4 \alpha_g \pi^2 (1 + \ln 2). \end{aligned} \quad (\text{A20})$$

The second part in Eq. (A19) yields

$$\int_{\alpha_g N \ln 2}^1 d\Omega P(\Omega)|_{Q < 1} = 4 \ln 2 \alpha_g^2 \pi^2 N \int_{\alpha_g N \ln 2}^1 d\Omega \frac{\text{arccot}(\alpha_g N \ln 2\Omega) - \arctan(\Omega/\alpha_g N \ln 2)}{2\alpha_g N \ln 2\Omega} = 4 \alpha_g \pi^2 G/2, \quad (\text{A21})$$

where $G = 0.916$ is the Catalan constant. Together, Eqs. (A20) and (A21) yield the result (10) from the main text.

b. *The limit $|\mu| \gg T$*

In the case $|\mu| \gg T$ we find that the rate Γ is determined by small energy and momentum transfer, $|\Omega|, Q < \alpha_g N |\tilde{\mu}|/2$.

$$\Gamma = 2T \int_0^{\alpha_g N |\tilde{\mu}|/2} d\Omega \left(\frac{\alpha_g N |\tilde{\mu}|}{2} \right)^{-2} \int_{|\Omega|}^{\alpha_g N |\tilde{\mu}|/2} \frac{dQ}{Q} = 8 \alpha_g \pi^2 |\mu| \quad (\text{A22})$$

Appendix B: The polarization operator in graphene

We use the dimensionless variables introduced in the preceding sections. Starting from the definition of the polarization operator in the Keldysh technique¹⁸

$$\Pi^R = \frac{i}{2} \int (d\varepsilon) \text{Tr} \left[\hat{G}^R(\varepsilon) \hat{G}^K(\varepsilon + \omega) + \hat{G}^K(\varepsilon) \hat{G}^A(\varepsilon + \omega) \right], \quad (\text{B1})$$

we obtain the following expressions for Π^R for arbitrary chemical potential and temperature,

$$\begin{aligned} \text{Im}\Pi^R &= \frac{TQ}{8\pi} \left\{ \frac{\Theta(1 - |\beta|)}{\sqrt{1 - \beta^2}} \int_1^\infty d\xi \sum_{s=\pm 1} \sqrt{\xi^2 - 1} \frac{\sinh(\beta Q)}{\cosh(\beta Q) + \cosh(s\xi Q - \tilde{\mu})} \right. \\ &\quad \left. - \frac{\Theta(|\beta| - 1)}{\sqrt{\beta^2 - 1}} \int_{-1}^1 d\eta \sqrt{1 - \eta^2} \frac{\sinh(\beta Q)}{\cosh(\beta Q) + \cosh(\text{sign}(\beta)\eta Q + \tilde{\mu})} \right\}, \end{aligned} \quad (\text{B2})$$

$$\begin{aligned} \text{Re}\Pi^R &= -\frac{TQ}{8\pi^2} P \int_{-1}^1 d\eta \int_1^\infty d\xi \sum_{s=\pm 1} \left\{ \frac{1}{\beta - s\eta} \sqrt{\frac{\xi^2 - 1}{1 - \eta^2}} \frac{\sinh(s\eta Q)}{\cosh(s\eta Q) + \cosh(s\xi Q - \tilde{\mu})} \right. \\ &\quad \left. - \frac{1}{\beta - s\xi} \sqrt{\frac{1 - \eta^2}{\xi^2 - 1}} \frac{\sinh(s\xi Q)}{\cosh(\xi Q) + \cosh(s\eta Q + \tilde{\mu})} \right\}. \end{aligned} \quad (\text{B3})$$

Here $P \int \dots$ denotes the principal value. The asymptotics for $|\tilde{\mu}| \gg 1$ in all relevant integration regions are given in Tab. I. For $|\tilde{\mu}| \ll 1$ they can be found in Ref. 18.

TABLE I. The asymptotics of the polarization operator in graphene for $|\tilde{\mu}| \gg 1$ in the different regimes from Eqs. (B2) and (B3). Here $I_\eta(z)$ denotes the modified Bessel function of the first kind.

	$ \beta < 1$		$ \beta > 1$	
	$Q \ll \tilde{\mu}$	$Q \gg \tilde{\mu}$	$Q \ll \tilde{\mu}$	$Q \gg \tilde{\mu}$
$\text{Re}\Pi^R$	$\frac{ \tilde{\mu} }{2\pi}$	$\frac{TQ}{16\sqrt{1-\beta^2}}$	$-\frac{T}{8\pi} \frac{I_1(Q)}{\beta^2} \frac{\tilde{\mu}^2}{Q}$	$-\frac{T}{4\pi\beta^2 Q}$
$\text{Im}\Pi^R$	$\frac{ \tilde{\mu} }{2\pi} \frac{\Omega}{\sqrt{Q^2 - \Omega^2}}$	$\frac{T}{4\sqrt{2\pi}Q} e^{-(1-\beta)Q}$, for $(1-\beta)Q \gg 1$	$-\frac{T}{16} \frac{Q^2}{\sqrt{\Omega^2 - Q^2}} \frac{\sinh(\Omega)}{\cosh(\Omega) + \cosh(\tilde{\mu})}$	$-\frac{T}{16} \frac{Q^2 \tanh \Omega}{\sqrt{\Omega^2 - Q^2}}$

Appendix C: Phase space of two particle scattering - the kinetic kernel

Finally we give the asymptotics of the kinetic kernel

$$\mathcal{K}(\Omega, Q) = 2T^2 e^\Omega \int_{-\infty}^{+\infty} d\xi \frac{\text{Re}[\text{sign}(1 - |\beta|)(\xi^2 - Q^2)]^{1/2}}{4 \cosh \frac{\xi - \Omega - \tilde{\mu}}{2} \cosh \frac{\xi + \Omega - \tilde{\mu}}{2}}, \quad (\text{C1})$$

for all integration regions.

TABLE II. The asymptotics of the kinetic kernel (C1) expressing the phase space for the thermal electrons participating at the scattering event.

$ \tilde{\mu} \gg 1$	$\beta < 1$		$\beta > 1$	
	$Q \ll \tilde{\mu}$	$Q \gg \tilde{\mu}$	$Q \ll \tilde{\mu}$	$Q \gg \tilde{\mu}$
\mathcal{K}	$4T^2 \Omega \tilde{\mu} (1 + \coth \Omega)$	$2T^2 \sqrt{2\pi} Q e^{-(1-\beta)Q}$	$T^2 \pi Q^2 e^{-(1-\text{sign}(\Omega)) \Omega }$	$T^2 \pi Q^2 e^{-(1-\text{sign}(\Omega)) \Omega }$
$ \tilde{\mu} \ll 1$	$\beta < 1$		$\beta > 1$	
	$Q \ll 1$	$Q \gg 1$	$Q \ll 1$	$Q \gg 1$
\mathcal{K}	$4T^2 \ln 2 e^{\beta Q}$	$2T^2 \sqrt{2\pi} Q e^{-(1-\beta)Q}$	$T^2 \pi Q^2 e^{-(1-\text{sign}(\Omega)) \Omega }$	$T^2 \pi Q^2 e^{-(1-\text{sign}(\Omega)) \Omega }$

Appendix D: Estimate of the scattering rate from Auger processes

The phase space for Auger processes is controlled by the parameter ε^*/Λ , which describes the curvature. To estimate

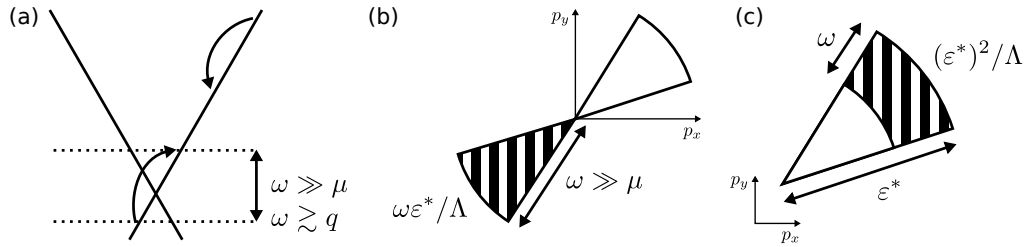


FIG. 8. (a) Auger process and (b) phase space for low energy electrons in the p_x - p_y plane; (c) phase space for high energy electron.

the contribution to the JSD from Auger processes, Fig. 8(a), we need the phase space for the high energy electron, which is given by $\sim \omega(\varepsilon^*)^2/\Lambda$ [Fig. 8(c)], and the phase space for the thermal low energy electrons $\sim \omega^2 \varepsilon^*/\Lambda$ [Fig. 8(b)]. Their product multiplied by the matrix element of scattering gives the following estimate for the JSD due to Auger processes,

$$P_{\text{Auger}}(\omega) = \frac{\omega^3 (\varepsilon^*)^3}{\Lambda^2} \left[\frac{|V(\omega, q)|^2}{|\omega^2 - q^2|} \right]_{\omega \gtrsim q} \sim \frac{(\varepsilon^*)^3}{\Lambda^2 \omega}. \quad (\text{D1})$$

Comparing P_{Auger} with P due to intraband transitions we find that for $\omega \gtrsim T(T^{1/3}\Lambda^{2/3}/\varepsilon^*)^2$, Auger processes dominate. However, if this threshold lies beyond the particle energy ε^* we can neglect them, i.e. for $\varepsilon^* \lesssim \Lambda(T/\Lambda)^{5/9}$. This applies irrespective of the relation between T and μ , provided $\omega \gg |\mu|, T$.